

MODIFIED MATRIX PENCIL ALGORITHM FOR TERMITE DETECTION WITH HIGH RESOLUTION RADAR

N. W. D. Le Marshall

University of NSW@ADFA
Australia

A. Z. Tirkel

Scientific Technology
Australia

Abstract—Non-invasive termite detection avoids damage to the structure under investigation. In this paper, we present the design and simulation of a hybrid radar array, with sub-arrays designed for both close range imaging and wide-area direction of arrival (DOA) processing for non-invasive termite detection. This radar array achieves wide area detection via novel modifications to the Matrix Enhanced Matrix Pencil algorithm and array transformation and achieves high resolution imaging through near field beam-steering from a large random array. The array hardware is designed to be implemented using available technology and low cost electronics.

1. INTRODUCTION

Our research over a number of years has been to detect termites presence or otherwise termites within the structure of buildings. This has led to a successful device developed by our group and commercialized by our group and by Termatrac[®] [1].

Termites are insects between 5 mm and 15 mm in length [2]. They digest vegetable matter for both nutrition and nest building. Unfortunately, several species have an affinity for timber used in building construction, leading to billions of dollars in structural and

Received 9 June 2010, Accepted 23 July 2010, Scheduled 10 September 2010

Corresponding author: N. W. D. Le Marshall (nick.lemarshall@student.adfa.edu.au).

cosmetic damage every year [3]. Non-invasive methods of detecting their presence are advantageous.

The Termatrac[®] device is a 24 GHz radar sensor that can detect termite activity behind a wall, floor or ceiling, but its area of coverage is limited to a single narrow beam, and imaging is not supported. It detects changes in the phase and magnitude of a RADAR signal which is transmitted towards the volume of interest.

Other methods of non-invasively detecting termites such as vibration sensing and gas detection have been proven less effective than movement detection via RADAR.

In this paper, we describe a novel hybrid 24 GHz RADAR array and imaging algorithm that we have developed, which provides the ability to scan a large area (up to 45 degrees from boresight) at a distance of about 1 meter. The array will be capable of indicating areas that have probable termite presence and also image at close range (around 100 mm), providing detailed information about locations and movements of individual insects. This array and algorithm will be able to indicate the direction of travel of the insects, their numbers and in some cases, the species.

The imaging of termites is a challenging problem. The signals scattered from termites are very weak whereas the structures where they inhabit tend to absorb or reflect signals strongly. We separate the changing termite signals from the clutter via a 0.1 to 10 Hz band pass filter, a technique which has been proven over years of field experience to pass the relevant signals. Without the filter the clutter will be larger than the termite signals by 60 dB or more. Movement of the instrument results in an increase of moving clutter in the RADAR signal and reduces the effectiveness of this filtering.

To maintain an acceptable SNR (at least 10 dB) from such a small target insect requires that the range from the imaging device to termite be short. The short range results in the insects being in the near field [4] of the RADAR array, which causes additional difficulties. Almost all imaging algorithms are designed for the far field where wave fronts can be approximated as planar. These algorithms, such as MUSIC [5] and ESPRIT [6], derive their rapid computation methods from spectral analysis of signals with static frequencies, a technique that is only appropriate where the phase gradients do not alter across the plane of the array, which is not the case in the near field. Techniques that enable far-field estimates to be corrected for near field curvature such as path-finding [7] and multiple small sub-arrays [8] have also been investigated and found inappropriate for this application as discussed in Section 1.

The signals received by the array are coherent due to the short

time of flight of the signals (approximately 1 ns for the imaging array and less than 10 ns for the DOA array). The autocorrelation of the signals is not appreciably altered by any phase and amplitude noise over such a short time span. For example, a 24 GHz VCO might display a phase noise of -140 dBc at 10 MHz offset which corresponds to 100 ns path length [9]. The amplitude noise is also similarly well below the noise floor for our application. Coherent signals further limit our choice of algorithm as the most commonly used algorithms; ESPRIT and MUSIC by default require incoherent signals. Techniques for creating incoherent signals from coherent signals such as forward-backward averaging [10] reduce the number of effective array elements lowering the resolution, SNR and maximum number of targets detected.

The paper is organized as follows: Section 1 explores the reasons for the selection of our hybrid array and algorithm. Section 2 describes the Matrix Enhanced Matrix Pencil (MEMP) algorithm and our modifications. In Section 3, array transformations to optimize various array parameters are explored. Section 4 explores our cancellation algorithm for near field and large numbers of targets. Section 5 shows the results of array simulations with the modified MEMP algorithm. Finally, Section 6 describes our method for near field imaging and simulation results.

2. ALGORITHM AND ARRAY GEOMETRY SELECTION

In order to meet the dual goals of far field DOA estimation and near field 3D imaging a hybrid array and algorithm were selected. A hybrid approach enables optimal performance in both environments.

The far field is defined as the region where the range to the target is greater than $D^2/wavelength$ where D is the largest dimension of the array. In our case, the entire array has dimensions of approximately 300 mm on a side, and hence the far field boundary occurs at 7.5 meters (for the 24 GHz design frequency). The near field encompasses the region between the array and a range of 1/10th of the far field range, or 750 mm. Significant wavefront curvature occurs within the near field zone. The zone between the far and near fields (750 mm–7.5 m) is known as the transition zone where curvature is present, but not as significant. These divisions are somewhat arbitrary, as the degree of curvature changes gradually throughout the range.

The Matrix Enhanced Matrix Pencil (MEMP) algorithm [11] was selected for the far field DOA algorithm. As outlined above, very few algorithms provide the capability to function with only a single snapshot, native processing of coherent signals and super resolution

accuracy.

When near-field targets are present, far-field algorithms will either produce incorrect estimates of these targets or fail to detect these targets entirely. This issue is particularly prevalent when both far and near field targets are in the field of view. In this case, far-field algorithms will most commonly report only the far field targets, failing to identify near field targets of similar or greater magnitude [12].

In the case of the MEMP, it was found that the presence of near field targets with equal or less amplitude to the far field targets did not affect the MEMP estimation of far field target location. Techniques such as path following [7], which are designed to compensate for incorrect target location estimates, cannot function when the DOA algorithm fails to resolve targets. An alternative technique of breaking the array into smaller sub-arrays does reduce the curvature, but individual sub-arrays will be much less effective than an algorithm using results from the entire receive array.

To overcome these problems, we choose to use beam forming [13] (specifically focusing) for our near field 3D imaging. We align the phases of signals arriving at all receiver elements from a point in 3D space to analyze the field at the target point. Focusing does not rely on the plane wave assumption and hence is not affected by wavefront curvature.

In order to support both far-field DOA and near field 3D imaging we have developed a hybrid array geometry. The hybrid array contains three distinct regions (Figure 1). A sparse randomly positioned receive array for high resolution near field (100–150 mm range) imaging operation and a dense uniform rectangular receive array for wide angle use beyond the near field (> 750 mm range) operation as required by the MEMP algorithm. A small transmit array is used as illuminator for both situations. The smaller central receive array has dimensions of 50 mm on a side, resulting in a far-field range of 200 mm.

The sparse random array geometry is preferred for our beam-forming network as the minimal reduction in resolution compared to a regular array of the same size with fewer array elements offset by a considerable improvement in ease of implementation and reduction in complexity.

A large array with a range of element spacing has a reduced alias response because many of its elements will be more closely spaced than those in a uniform array. In a uniform array spacing is limited due to the size of the support electronics whereas in a randomly spaced array, these support electronics can be placed between widely spaced elements.

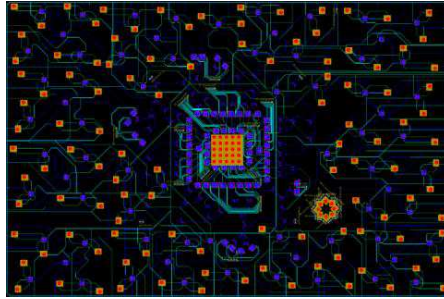


Figure 1. Hybrid array. Three distinct regions can be observed; a central dense receive array for far field use, a peripheral random receive array and a small transmit array at lower right of the figure.

3. MEMP ALGORITHM

Signals received by a regular rectangular array with element spacing (Δ_x, Δ_y) can be modeled using Equation (1):

$$x(m : n) = \sum_{i=1}^I A_i \exp(j\gamma_i + 2\pi m \Delta_x \sin\theta_i \cos\varphi_i + j2\pi n \Delta_y \sin\theta_i \sin\varphi_i) \quad (1)$$

where i is the signal from array elements 1 to I ; A_i is the amplitude; γ_i is the phase; φ_i is the elevation; and θ_i is azimuth.

In the MEMP algorithm, the signal sample values are assembled into an enhanced matrix using a partition and stack process [11]. A Singular Value Decomposition (SVD) is used to estimate the number of targets present. This establishes the signal and noise subspaces within the data matrix. The signal subspace eigenvalues are determined by matrix inversion and used to estimate the azimuths and elevations of all the targets in the signal subspace via a pairing algorithm [14]. Amplitude and phase information can also be estimated by this process.

In order to optimize the Matrix MEMP for our application we have made a number of changes. In a rectangular array with M by N elements, the standard MEMP algorithm supports a maximum number of target, which is equal to either $M - 1$ or $N - 1$, whichever is less. In some situations there may be more targets in the field of view than elements in the array, so we developed an algorithm to resolve many more targets.

The MEMP works well in the context of an ideal array, but using with real arrays requires compensation to reduce the effects of several imperfections. One major issue is mutual coupling, where the signals

transmitted from one element alter those of surrounding elements.

Mutual coupling is particularly significant for our array as the receiver elements for the matrix pencil are required to be closely spaced. The coupling of signals from nearby elements into the received signal forms multipath components.

The received voltage at the p th element of an array from the i th signal is:

$$x(p) = \sum_{i=1}^I A_i e^{(j\gamma_i + R_{i(p)})} \quad (2)$$

where $0 \leq p \leq P - 1$, $j = \sqrt{-1}$. A_i and γ_i are the amplitude and phase of the i th target, and $R_{i(p)}$ is the range between the i th signal source and array element i . With mutual coupling, this becomes:

$$x(p) = \sum_{i=1 \dots I} \left[A_i e^{(j\gamma_i + R_{i(p)})} + \sum_{k=1 \dots I, k \neq i} C_{i,k} A_i e^{(j\gamma_i + R_{i(p)})} \right] \quad (3)$$

where $C_{i,j}$ is the coupling factor between the i th and j th element. The coupling factors result from electrostatic dipole coupling, inductive near field coupling, PCB surface wave coupling, and other waveguide modes induced in the substrate.

There are various actions that we can take to reduce the level of coupling. For instance, a simple calculation using single aperture experimental data [15] indicates that angling the array apertures at 45° relative to the rectangular lattice orientation can reduce coupling by up to 8 dB. Also, using the minimum possible substrate thickness, determined by manufacturing capabilities, reduces surface wave coupling.

An array transformation (detailed below) can be used to cancel these coupled components [16]. Determination of the optimal compensation matrix can be difficult, as it requires knowledge of the coupling coefficients. Measurement of the coupling coefficients requires to treat the array as a multiport network with all non-driven ports (such as measurement ports) treated as though terminated by open circuits. This is not possible without altering the design of the array which will in turn alter the coefficient that we are measuring. An alternative is to perform a full method of moments (MOM) simulation of the array. We would expect this to provide an accurate estimate of the coupling coefficients. Even so, the coefficients should be checked against a physical array.

4. ARRAY TRANSFORMATIONS

Compensation can be achieved using an array transformation [17]. These transformations can only be applied to signals arriving from a limited range of angles at once, known as an angular sector. Out of sector targets are not properly transformed, potentially disrupting the in-sector targets whose properties we are attempting to estimate. In order to reduce this effect, our algorithm permits selective spatial filtering of out-of-sector targets [12].

Beyond a certain sector size, the accuracy of the transformation declines resulting in erroneous DOA estimates, and hence the sector size is limited. We have selected the sector size using simulations to determine the maximum sector size which maintains DOA accuracy to within a few degrees. In our case, azimuthal sectors of $\pi/2$ and elevation sectors of $\pi/4$ were chosen.

The array transformation matrix is calculated as the least mean squared solution to:

$$T = \arg \min_T \|TA_R(\phi_i, \theta_i) - A_V(\phi_i, \theta_i)\|_F^2 \quad (4)$$

where A_R and A_V are the array manifolds from a set of angles generated either from simulation or calibration data for the real rectangular and virtual rectangular array respectively, and T is the transformation matrix which is the solution to the above problem using a least mean square algorithm.

The transformation matrix is employed as follows:

$$a_V = Ta_R \quad (5)$$

where a_R is the real array response, and a_V is the virtual array response. The DOA algorithm is then applied to the virtual array response.

5. CANCELATION ALGORITHM

Out-of-sector signals can interfere with in-sector signals when the matrix transformation is employed. As a result, we need to pre-filter the data before transformation.

Traditional methods of spatial filtering involve multiplying data from each element of the array by complex filter coefficients before summing the resulting products. The coefficients are selected to phase align the signals from the look direction of the filter. This maximizes the sum of the filtered element responses to signals in the look direction and minimizes the sum due to signals from other angles. This method is not applicable when using the MEMF as it alters or removes phase information which the MEMF requires for its DOA estimates.

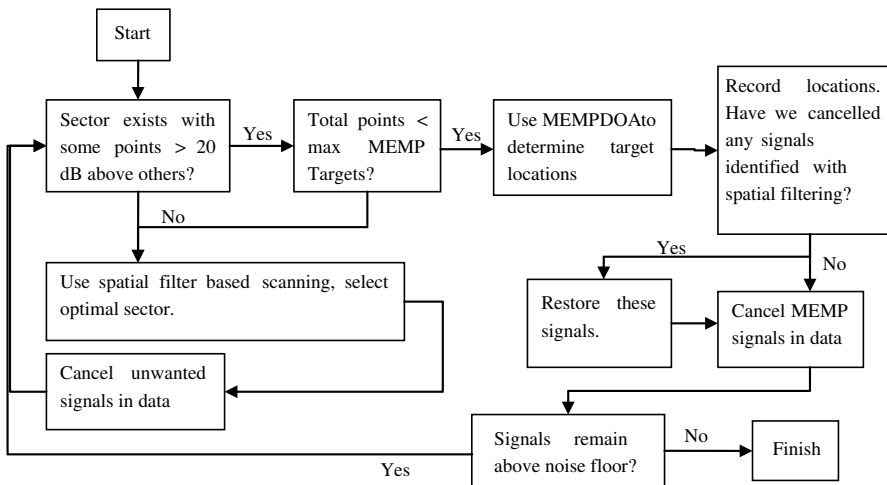


Figure 2. Basic flowchart for DOA/cancellation algorithm.

Our algorithm is designed to selectively suppress out-of-sector signals to enable an accurate matrix transformation and to filter in-sector signals to enhance the MEMP effectiveness. It relies on detecting signals via spatial filtering and then suppressing them by injecting signals of equal amplitude but opposite phase.

Simulations have shown that the magnitude of the out-of-sector signal should be at least 20 dB less than the in-sector signals [17] to avoid interference. We have developed a cancellation algorithm to address this issue. The algorithm is detailed in full below, and a summary of the algorithm is shown as a flowchart in Figure 2.

Using the method of [18] a narrow 2D filter in both elevation and azimuth is designed. This filter is swept through a fixed grid of azimuth/elevation positions, and the filter output is recorded. These outputs are used to build a map of the power levels seen by the array at various angles. The positions can be written as:

$$S = \left\{ (az, el, p) \left| \begin{array}{l} az = (\Delta_{az}, 2\Delta_{az}, \dots, 2\pi), \\ el = \left(\Delta_{el}, 2\Delta_{el}, \dots, \frac{\pi}{2} \right) \end{array} \right. \right\} \quad (6)$$

$$P = \{P_i \in S | P_i \geq \text{Power}_n + 20 \text{ dB}\} \quad (7)$$

where S is the set of azimuth, elevation and power triples, and P is the set of triples with significant power. Within the triple, az is the azimuth; el is the elevation; p is the power level; Δ_{az} is the azimuth stepping; and Δ_{el} is the elevation stepping. Power_n is the power at the noise floor. As can be seen in Equation (7), any point with power less

than 20 dB above the noise floor is discarded. We then have a list of angles (P) that contain appreciable power levels and possible targets.

Although the initial spatial filter sweep provides some information about the location of the targets, the MEMP is essential to achieve super-resolution estimates. During the cancellation stage we can achieve the required 20 dB suppression without needing super-resolution accuracy.

The next step is for the algorithm to select the optimal sector in order to proceed. We first rank the data points by the power received from that angle. We then select a sector containing the angle (bearing) with the highest power, which in addition maximizes the number of angles from the list P (in Equation (7)) that are within this sector.

We now have a set of data points D that are within the optimal sector. We then determine the set of points with the maximum power level (P_{\max}) from the set of points P and select a sector that contains at least one element from P_{\max} and the maximum number of points from P . This sector contains the points D_i ($D_i \in P$, $P_{\max} \in D_i$).

Once the sector is determined, the algorithm selects, from the list, all data points outside the sector that have power levels within 20 dB of the data points within the sector. The power arriving from these angles must be reduced to suppress interference with in-sector signals.

In the neighborhood of each interfering signal we perform a gradient based search to determine, more accurately the azimuth, elevation, phase and range of the interfering signal. We can then inject a cancellation signal that has the same bearing and power but with opposite phase. If necessary we can also cancel the lowest magnitude in-sector signals if there are more signals than what the MEMP can resolve.

Once cancellation is completed, the DOA algorithm can estimate the in-sector signals and record their locations for final output.

A new iteration can then begin. In subsequent iterations, MEMP based estimates of signal properties can be used to cancel signals more precisely than the spatial filter based estimates. Iterations will continue until all signals above the noise floor have been estimated by the MEMP.

The number of targets that can be correctly detected using this method depends primarily on the accuracy of signal property estimation. Estimation accuracy determines the magnitude of the cancellation. Simulations have shown that our spatial filter based parameter estimation is sufficiently accurate to provide the required 20 dB of cancellation.

Figures 3 and 4 show simulations of the cancellation algorithm. In this simulation, the algorithm correctly determines the location of an

interfering signal and cancels it with the signal of interest left intact.

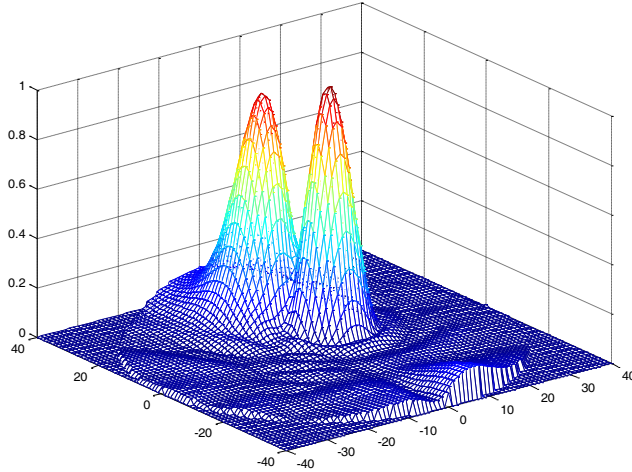


Figure 3. Desired target (left) and interfering target (right). x and y units are in degrees azimuth and elevation. z units are in arbitrary linear magnitude units.

6. DOA ARRAY RESULTS

In order to assess the performance of the DOA algorithm, we used captured data of termite movement to create a simulated RADAR environment.

We set up two containers with food and nest material respectively. The containers were connected by a plastic tube, and termites were encouraged to travel between the two. The plastic tube is a reasonable analog of the mud-tubes where termites inhabit. The images of termites traversing the tube were captured, via a video camera. The video footage is converted to still images, where each frame is separated by 0.1 seconds. This results in a 10 Hz frame rate, which is the expected frame rate of our RADAR array. A frame from the video footage is shown below in Figure 5.

Image processing was used to detect the location of termites within the tube in each of the 5200 frames in the video sequence. A simulated RADAR environment was created for each frame, and targets with properties equivalent to a termite were placed at the points corresponding to the termite locations within the images. For each frame, an array simulation (including the MEMP algorithm) was

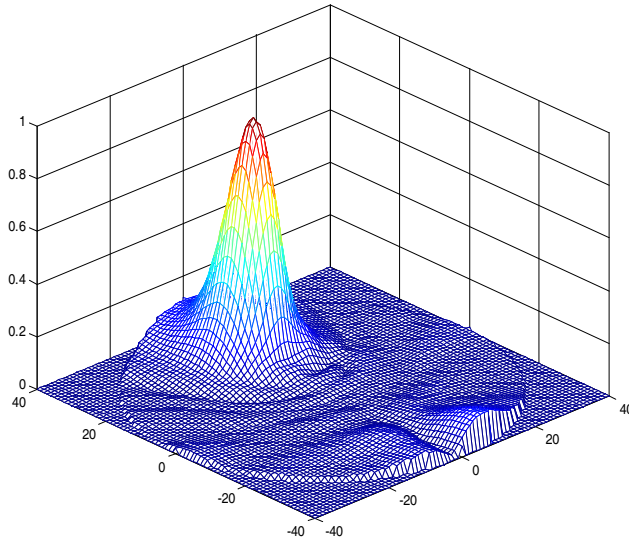


Figure 4. Result after suppression of interfering target. x and y units are in degrees azimuth and elevation. z units are in arbitrary linear magnitude units.

performed, and the resulting target location estimates were recorded.

Termites move at a maximum velocity of 5 mm per second. In the video the number of termites in a frame varied between 0 and 8. The video processing did produce some over and under identification



Figure 5. Video frame showing termites moving along 10 mm diameter polymer tube.

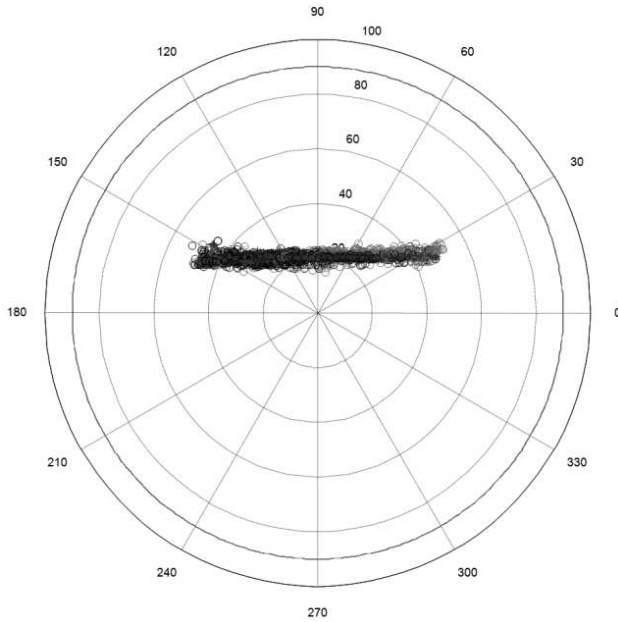


Figure 6. All termite location estimates for 5200 frames of video.

of termites. In these situations it was found that the disposition and orientation of the termites justified this behavior. Examples of this include two termites adjacent to each other or a single termite being identified as two targets, one for the head and one for the abdomen.

Figure 6 depicts the combined results of these simulations and was produced by plotting the target locations from all frames onto a single polar axis. As can be seen, almost all termites were correctly located within the tube. Of the 8,000 termite locations identified only 3 low confidence targets were incorrectly identified as outside the plastic tube. Some low confidence targets (not shown) are those targets that the MEMP identifies but with some irregularity in their phase gradients, most likely as a result of imperfect matrix transformation.

7. IMAGING SUB-ARRAY

For imaging at ranges less than 620 mm, wavefront curvature is significant, and we use array focusing [13] to produce high resolution 3D images of targets. Focusing does not rely on the plane wave assumption. It aligns the phases of signals arriving at the array from a point in 3D space, to analyze the field at the target point.

Termites move relatively slowly (typically 5 mm/sec), and a 10Hz frame rate is sufficient for realtime imaging. The number of calculations required by our imaging algorithm is determined by the number of voxels in the image. A 3 mm on-a-side voxel was chosen as appropriate for the analysis of termite signals as it is commensurate with the size of the insects and the resolution of our array (see below). The number of 27 mm^3 voxels in a hemisphere of radius 620 mm is 18.9×10^6 and is an upper bound.

Imaging requires a large amount of computational resources, hence we need to ensure that the amount of calculation required is possible in a portable device. By pre-computing phase shifts, required for beam-forming, only one multiply accumulate (MAC) operation is required for each sub-array element per frame per voxel. A MAC is a basic computational operation that enables us to compare DSP performance between architectures and algorithms.

The minimum number of sub-array elements is determined by acceptable alias suppression (6 dB, Figure 7), which in our case, is between 64 and 128 array elements. The total number of calculations required is then 20 GigaMAC/sec which is possible using low cost digital signal processing (DSP) that is currently available [19].

Another requirement is an acceptable spatial resolution, which depends on aperture area. Our simulations use an imaging sub-array of

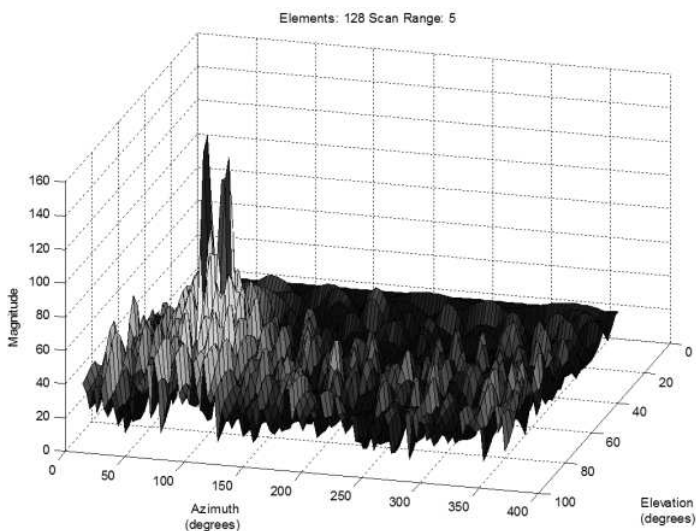


Figure 7. Full hemisphere scan at 62 mm range. Both targets are at range 62 mm and elevation of 55° . Target azimuths are 70° and 85° .

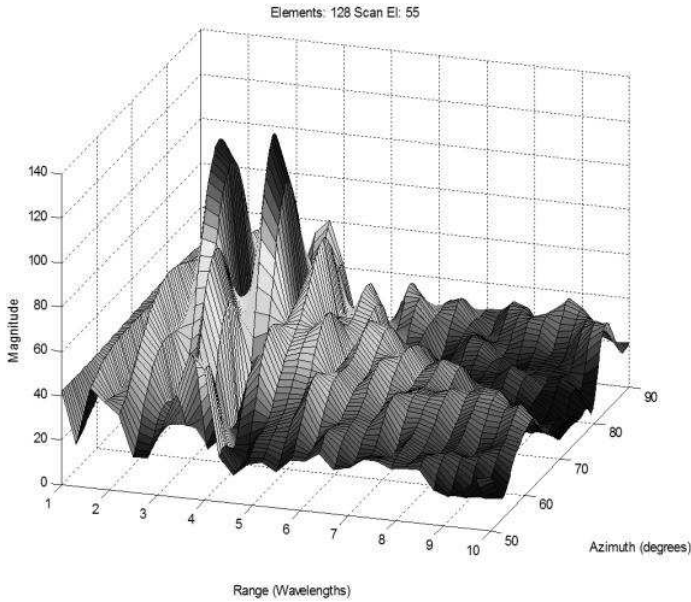


Figure 8. Magnitude of returns from beamforming over range. 2 targets placed at 36 mm and 50 mm, azimuths are both 70° , with elevations of 55° . Scan is 2-dimensional from $55\text{--}90^\circ$ azimuth and 1–120 mm range at 55° elevation.

128 elements, distributed randomly over a square area of approximately 300 mm on a side. This sub-array has achieved a range resolution of better than 14 mm and a cross-range resolution of better than 16 mm, up to a range of 300 mm. Resolution was defined by the Rayleigh criterion. Figure 7 shows the targets in cross-range. Figure 8 shows two targets closely spaced in range.

Figure 8 highlights the range resolution using our array with focusing. We can compare this to well-known methods such as a Fourier based time-frequency process (FMCW) using the allowable Industrial Scientific and Medical (ISM) band (24.000–24.250 GHz), which has a range resolution of 600 mm. The range resolution achieved in Figure 8 is at least 50 times better. Methods that are resistant to near field curvature such as spectrograms and wavelet methods have even poorer resolution.

Table 1 summarizes the azimuth and elevation cross-range resolution performance of the DOA and 3D imaging sub-arrays at the two ranges at which the hybrid array is designed to operate.

Table 1. Cross-range resolution of DOA and 3D imaging sub-arrays. All dimensions in millimetres.

Range (mm)	Azimuth resolution (mm)		Elevation resolution (mm)	
	DOA	Imaging 3D	DOA	Imaging 3D
120	22	13	53	11
1200	2–11	76	8–32	76

It was found that the DOA sub-array performs reliably for ranges beyond 620 mm (despite the curvature), and the 3D imaging sub-array is suitable for ranges less than 620 mm. The DOA and 3D image processing can be implemented in currently available hardware [19]. The cross-range resolution of the DOA sub-array, operating at 1200 mm range, is inadequate for resolving individual termites. The 3D imaging sub-array is capable of resolving individual termites, focusing curved wavefronts in the near field, and providing adequate range resolution, without a frequency sweep. Therefore, the DOA array can be used to localize activity and direct the inspector to such an area, where the imaging sub-array can provide a high resolution 3D image.

8. CONCLUSIONS

In this paper a hybrid radar array, designed for long range non-invasive detection of termites and short range high resolution imaging of termites, is described. This radar array uses 24 GHz sensors and a modified DOA algorithm (MEMF) to resolve arbitrary numbers of targets. Results show that the modified DOA algorithm is capable of estimating the azimuths and elevations of moving termites over a wide area. High resolution images of termite activity are obtained by a 3D imaging sub-array using focusing.

ACKNOWLEDGMENT

The authors acknowledge the Australian Research Council for their financial support, under Linkage Grant LP0669638, the University of New South Wales at the Australian Defence Force Academy for infrastructure support, Termatrac Pty Ltd and Scientific Technology Pty Ltd. (industrial partners) for their facilities and equipment for this project. The authors further acknowledge Donald Fraser and Joseph Lai for helpful suggestions in preparing this manuscript.

REFERENCES

1. Termtrac Pty Ltd., Termatrac Corporate Website, [Online], <http://www.termatrac.com>.
2. Abe, Y., D. E. Bignell, and T. Higashi, *Termites: Evolution, Sociality, Symbioses, Ecology*, Springer, 2000.
3. Caulfield, R. and P. Daly, "An analysis of termite damage in Sydney and Melbourne," *Archicentre Limited*, Hawthorn, Victoria, Australia, 2006.
4. Alliance for Telecommunications Industry Solutions, American National Standard T1.523-2001, Telecom Glossary 2000, 2001.
5. Schmidt, R., "Multiple emitter location and signal parameter estimation," *IEEE Transactions on Antennas and Propagation*, Vol. 34, No. 3, 276, March 1986.
6. Roy, R. and T. Kailath, "ESPRIT — Estimation of signal parameters via rotational invariance technique," *IEEE Transactions on Acoustics, Speech and Signal Processing*, Vol. 37, No. 7, 984–995, July 1989.
7. Park, D. H., G. T. Park, and K. K. Lee, J. H. Lee, "Algebraic path-following algorithm for localising 3-D near-field sources in uniform circular array," *Electronic Letters*, Vol. 39, No. 17, August 21, 2003.
8. Miller, E. L. and A. Sahin, "Object detection using high resolution near-field array processing," *IEEE Trans. on Geoscience and Remote Sensing*, Vol. 39, 136–141, 2001.
9. Hittite Microwave Corporation, "HMC533LP4 datasheet," Massachusetts, USA, http://www.hittite.com/content/documents/d-ata_sheet/hmc533lp4.pdf.
10. Bachl, R., "The forward-backward averaging technique applied to TLS-ESPRIT processing," *IEEE Transactions on Signal Processing*, Vol. 43, No. 11, 2691–2699, November 1995.
11. Hua, Y., "Estimating two-dimensional frequencies by matrix enhancement and MEMP," *IEEE Trans. on Signal Processing*, Vol. 40, No. 9, 2267–2280, September 1992.
12. Le Marshall, N. W. D. and A. Z. Tirkel, "The application of the MEMP and beamforming to determine the presence of termites in situ," *IEEE EUROCON Proceedings*, 1568–1572, 2009.
13. Van Trees, H. L., *Detection, Estimation, and Modulation Theory, Part IV, Optimum Array Processing*, Wiley, New York, 2002.
14. Sarkar, T. and S. Burintramart, "Target localization in three dimensions," *Advances in Direction of Arrival Estimation*,

- S. Chandran (ed.), Chapter 5, 87–102, Artech House, Boston, USA, 2006,
15. Humphrey, D. E. J. and V. F. Fusco, “A mutual coupling model for microstrip patch antenna pairs with arbitrary orientatio,” *Microwave and Optical Technology Letters*, Vol. 18, No. 3, 1998.
 16. Kyungjung, K., T. K. Sarkar, and M. S. Palma, “Adaptive processing using a single snapshot for a nonuniformly spaced array in the presence of mutual coupling and near-field scatterers,” *IEEE Transactions on Antennas and Propagation*, Vol. 50, No. 5, 582–590, May 2002.
 17. Friedlander, B., “Direction finding using an interpolated array,” *International Conference on Acoustics, Speech, and Signal Processing*, Vol. 5, 2951–2954, 1990.
 18. Dessouky, M., H. Sharshar, and Y. A. Albagory, “An approach for low sidelobe beamforming in uniform concentric circular arrays,” *Wireless Personal Communications: An International Journal*, Vol. 43, No. 4, 1363–1368, 2007.
 19. Brown, G., “Spartan-DSP takes aim at affordable DSP performance,” *DSP Magazine*, No. 3, 8–9, April 2007.